An ARIMA-based Statistical Approach for Multi parametric Earthquake precursor study in North East India.

By

[1]Partha Sarkar, [2]Bijoy Dutta, [1]Sanjay K. Prajapati, [3, *]P. N. S. Roy, [4]Sanjit K. Pal and [1]O. P. Mishra

[1]National Centre for Seismology – Ministry of Earth Science, New Delhi-110003, INDIA

[2]Dept. of Earth Sciences, Indian Institute of Technology Kanpur, Uttar Pradesh-208016, INDIA

[3]Dept. of Geology & Geophysics, Indian Institute of Technology Kharagpur, West Bengal-721302, INDIA

[4]Dept. of Applied Geophysics, Indian Institute of Technology (Indian school of Mines) Dhanbad, Jharkhand-826004, INDIA

[*]Corresponding author's e-mail: pareshsr@gg.iitkgp.ac.in

Phone: +91-3222-281790. FAX: +91-3222-281790.

An ARIMA-based Statistical Approach for Multi parametric Earthquake precursor study in North East India.

ABSTRACT

Investigating non-tectonic phenomena for earthquake forecasting constitutes a central area of interest for researchers. Located globally, it is worth noting that North-East India and its environs exhibit heightened seismic activity. This links to the intricate configuration of tectonic plates in the region, contributing to the increased occurrence of earthquakes. The current investigation focuses mainly on a short-term multi-parametric earthquake precursor study using variations in total electron content (TEC) values derived from GNSS (IGS) measurements, atmospheric temperature (AT) and relative humidity (RH) and the fractal correlation dimension (Dc) in the context of three significant earthquakes. The ionospheric Total Electron Content (TEC) anomaly is a dynamic phenomenon that exhibits spatial and temporal characteristics influenced by the clustering behaviour of the medium. We can aptly characterize the clustering of the medium by employing the fractal correlation dimension. The correlation indicated between the lower Dc value for the earthquake data catalogue from 2014 to 2021 and the variable ionospheric TEC value of North-East India. This study is essential role in understanding the Lithosphere Atmosphere Ionosphere Coupling (LAIC) mechanism and the seismo-ionospheric coupling before an earthquake. The study effectively establishes a correlation between two parameters, namely the fractal correlation dimension and TEC value measurements. This correlation aids in the identification of potential timing and prominent regions with high seismic activity, specifically for strong-magnitude earthquakes. In addition, a statistical model known as Auto Regression (AR) and Moving Average (ARIMA) helps to authenticate the observed anomaly as having a seismogenic origin.

Keywords: Earthquake precursor studies, Fractal correlation dimension, Seismicity analyses, Statistical analyses, Total Electron content (TEC), Atmospheric temperature, Relative humidity.

1. Introduction

Numerous investigations led to the understanding that the seismo ionospheric coupling mechanism is a pre-seismic signature, employing GNSS-derived vTEC data. During the seismic event in Alaska 1964, the Seismo-Ionosphere anomalies indicate notable observations. In their reports Davies and Baker, (1965), and Leonard & Barnes, (1965) indicate these observations. Liu et al. (2004) show a sharp decrease in Total Electron Content (TEC) values before the Taiwan earthquake. Furthermore, it is worth noting that an augmented Total Electron Content (TEC) measurement can detect within the western region of the seismic event in Sumatra, Indonesia, on December 26, 2004, Otsuka et al. (2006). Nevertheless, it is worth noting that multiple occurrences support the presence of positive and negative ionospheric anomalies preceding a mega-earthquake. The Ionosphere is currently the subject of extensive deliberation regarding the resolution of TEC anomaly. The seismic activity in the region has been steadily increasing over the past few weeks.

The seismo-tectonic nature of North-East India is highly intricate, characterized by a multitude of significant and dynamic faults. These faults have experienced various seismic activity, including moderate to large earthquakes. Notable examples include the Assam earthquake of 1950, the Shillong earthquake of 1897, the 1945 Kopili earthquake and the recent 2011 Sikkim earthquake, the 2016 Manipur earthquake and the recent 2021 Sonitpur earthquake, among others, within the region. In North East India, several experiments have been conducted to assess the likelihood of a high-magnitude earthquake. These experiments, as documented by Liperovsky et al. (2000), Silina et al. (2001), Singh and Singh (2007), Zhou et al. (2009), Dogan et al. (2011), and Pundhir et al. (2014), have contributed to our understanding of seismic activity

in the area. Recently, investigations in this area have reported the precursor signals of outgoing long wave radiation (OLR) associated with two seismic events of M=6.7 and M=6.9, which took place in January and April of 2016, respectively.

Researchers are exploring multiple concepts to establish a correlation between crustal tectonic activity and the ionosphere layer to understand the Lithosphere Atmosphere Ionosphere Coupling Mechanism (LAIC). This endeavour aims to investigate potential precursors that may indicate the occurrence of high-magnitude earthquake events. Based on the 'Peroxy' defect hypothesis proposed by Freund et al. 2009, it suggests that the strength of rock material can improve, as deviatoric stress concentration increases. Consequently, this can lead to compression of the rocks, accompanied by the release of energy through the presence of positive holes within the fault. The increasing radioactivity of the atmosphere leads to an increase in electrical conductivity within the near vicinity of the ground atmosphere. Radon gas emission happens from the earth's crust, a vital source of ions to the atmosphere (Hoppel et al., 1986). O_2 having the least ionisation potential, eventually becomes the most favourable candidate to ionise in the atmosphere (O_2^+). The researchers report that the ionisation rate at a flat rock surface with small edges is 10^7-10^9 s^{-1} cm^{-2} (Freund 2010, 2013, Freund et al., 2017). This ionization phenomenon will eventually lead to upward migration of the evolved ion clusters. During the upward movement, the +ve ion clusters act as nuclei for condensation to take place for the formation of water droplets.

Due to this condensation, latent heat releases, leading to a significant reduction (-ve) in relative humidity. The radiated latent heat will give rise to a +ve air temperature (AT) anomaly and land surface temperature (LST) anomaly. As this +ve ion cluster reaches the lower part of the ionosphere, it will create a deficiency of vTEC over the earthquake preparation zone (EPZ). The 'peroxy' defect-derived microscopic phenomenon results in the macroscopic impact in the ionospheric total electron concentration. The observed phenomenon exhibits a spatio-temporal progression, resulting in a reduction in the concentration of electrons, thereby leading to

significant irregularities in the Total Electron Content (TEC) values. Following the findings of Liu et al (2004), (2006), (2009), (2010), Sharma et al (2010), Xu et al (2015) it is observed that the arrangement of particle bunches in the ground layer is a dynamic geological process that generates gaseous radon atoms, resulting in the formation of a distinctive electric field. The postulate of the presence of radon gas contributes to the occurrence of dual-phase phenomena due to atmospheric motion, generating acoustic gravity waves. The observed gravity wave disrupts the distinct particle clusters due to a deficiency in the Coulomb interaction and increases in the number of particles. Finally, the immense aggregation of particles within the subterranean stratum generated a vertical electrical field. However, following the orientation of this electric field for the Earth's surface, negative and positive electron fixation may be observed (Pulinets et al., 2002, 2004). In calculating the ionospheric Total Electron Content (TEC) anomaly analysis reports on the solar-terrestrial conditions, precisely the Solar flux $F_{10.7}$ scale and Geomagnetic storm Ap index. The solar flux is a measure of the radiation received from the Sun, determined by observing the radio noise emitted at a frequency of 28000 MHz (10.7 cm). The ionosphere is subject to the influence of geomagnetic indices, which measure the Earth's magnetic field state impacted by solar activity. To study the LAIC mechanism, we also analysed for the temporal variations of the Atmospheric Temperature (AT) and Atmospheric Relative Humidity (ARH) at two-meter height before the earthquake.

Understanding seismicity, a phenomenon that occurs in space and time, can be significantly enhanced by examining its scale invariance pattern. This analysis involves by utilizing fractal correlation dimension, a widely accepted technique in earth science (Turcotte et al., 1986). The Dc value exhibits a correlation with the spatial arrangement of the medium, which in turn has an indirect association with the propagation of radon within the medium. This ongoing investigation endeavours to anticipate and ascertain the state of crustal heterogeneity by establishing a correlation between the variations in ionospheric Total Electron Content (TEC) and the fractal correlation dimension of seismic activity associated with earthquakes. The

frequent incidence of seismic activity presents a remarkable opportunity to conduct a statistical analysis of the correlation between ionospheric anomalies and earthquakes. A statistical investigation "ARIMA model" was adapted to indicate the seismic origin of this ionospheric anomaly. The study focused on earthquakes with a magnitude of Mw ≥ 6.0 occurring between 2014 and March 2021 in the North-East region of India. An observation of a noteworthy decrease in the current Total Electron Content (TEC) value has been made based on the chosen ARIMA model. This finding provides conclusive evidence that supports the existence of a negative ionospheric anomaly.

2. Seismotectonic activity of the region

The investigation of TEC variation relates to the three significant seismic events that transpired on 13.04.2016, 17.11.2017, and 28.04.2021, respectively, within the eastern boundary zone and the Mishmi Himalayan zone. Observations indicate that North East India exhibits a significant level of seismic activity, rendering it one of the prominent regions in India in terms of seismicity. Based on the seismicity patterns observed in this region, it is evident that the Indo-Burman orogeny, the primary mountain belt along the Eastern boundary zone, plays a significant role in seismotectonic activity. The region is delineated by a many dynamic tectonic faults, thrusts, and diverse geological characteristics, as visually depicted in Figure 1. The Indo-Burma region exhibits a prominent N-S trending fold-thrust belt, occupying a geologically intricate tectonic zone characterized by oblique subduction towards the western boundary. In the Burma region, numerous active faults are observed (Le Dain et al., 1984). These faults result from the convergence and subduction of the Indian plate along the Indo-Burma arc (Mitchell and Mckerrow, 1975; Mitchell et al., 1981). The Sagaing Fault in the East and Mishmi thrust in the North are of utmost significance as key tectonic features. In our study area, the world's largest Bengal basin is located towards the far west of the Indo-Burman range, as noted by Chen and Molar in 1977. The Indo-Burma range exhibits additional tectonic structures, including the Naga Hills and the Kabaw faults.

The Northeastern corner of the study zone is home to a highly active area known as the Mishmi Himalayan zone. This zone exhibits a structural trend oriented towards the N-W direction. The region in question indicates the presence of overriding thrust faults that dip towards the north-west and south-east. These faults traverse the Himalayan and Burmese arc, as documented by Ni and York in 1978. The Mishmi thrust and Lohit thrust (Nandy et al., 1973) are the primary tectonic faults acknowledged within this geographical area. In this particular location, there is evidence of the frontal thrust (Mishmi) exerting pressure on the upper Assam valley. However, recent seismic activity indicates a notable occurrence of right-lateral shear within this area. In this region, the presence of various parallel ridges, valleys, and NW-SE trending Lohit thrust located in the eastern portion of the Mishmi thrust, as documented by Kayal et al. in 1987.

3. Data Analysis

To accurately determine the fractal correlation dimension value within an active seismic region, it is imperative to possess a comprehensive data catalogue. The data utilized in this study was obtained from the USGS (http://earthquake.usgs.gov) data catalogue spanning the years 2014 to 2021. This comprehensive dataset was employed for the purpose of constructing a thorough data catalogue aimed at quantifying the fractal correlation dimension. The GNSS derived ionospheric Total Electron Content (TEC) data has been acquired from the ftp://cddis.gsfc.nasa.gov site in IONEX format. The International GPS Service (IGS) provides global access to a comprehensive ionospheric database encompassing the Total Electron Content (TEC) values across the entire planet. The data pertaining to solar indices, specifically geomagnetic activity (Ap indices) and solar flux $_{F10.7}$, during the specified time frame for the three significant events (as presented in Table 1), has been gathered from the official website of NASA's Goddard Space Flight Center (https://omniweb.gsfc.nasa.gov). This collection aims to examine the seismic occurrences in their true form, devoid of any solar influence. The atmospheric Air Temperature (AT) and Relative Humidity (RH) data has been retrieved at the epicentral location by the Prediction of Worldwide Energy Resources (POWER) at 2m height

(https:// power.larc.nasa.gov/data-access-viewer). The retrieved dataset has a spatial resolution of 0.5º×0.5º.

4. Methodologies

4.1 Fractal correlation dimension (Dc)

The correlation integral procedure yields the correlation fractal dimension (Dc), which is contingent upon the subtle variations in clustering characteristics (Kagan and Knopoff, 1980; Hirata et al., 1989). The fractal correlation dimension is determined by evaluating the correlation integral, as proposed by Grassberger and Procaccia in 1983. This integral provides a consistent and precise measure, quantifying the proportion of points within the two-dimensional space. It is mathematically expressed as,

$$\boldsymbol{C(r) = \frac{2}{N(N-1)} \sum_{j=1}^{N} \sum_{i=j+1}^{N} H(r - r_{ij})} \quad (1)$$

In the context of calculating the value of D_C for a fractal set, the variable N represents the total number of pairs. The scale is denoted by r, while the distance between the points in the set is defined as r_{ij}. The estimation of r_{ij} is accomplished using the spherical triangle method, as elucidated by the previous researchers Roy and Ram (2006) and Roy and Padhi (2007). The symbol H is commonly referred to as the Heaviside step function in the field of seismology. Henceforth, the count of point pairs that exhibit a separation distance smaller than r is directly correlated to the function C(r) within the fractal ensemble. The system of points in a fractal set is being investigated through experimentation, with a particular focus on plotting these points in logarithmic coordinates. The logarithmic plot of Log C(r) as a function of Log (r) should exhibit a segment that appears linear, characterized by the slope D_C. This slope corresponds to the optimal fitting values of r, which represent the fractal dimension of the system as described in Equation 1.

The Fractal Analyzer (Roy and Gupta, 2015) was employed in order to calculate the fractal dimension value, taking into account the aforementioned considerations. The arrangement of the data catalogue follows the sequence of Year, Month, Day, Hour, Minute, Latitude, and Longitude. In this manner, the initial fifty data rows are selected and treated as a singular data window or set. Thirteen data windows have been utilized to estimate the Dc value across various time periods. The error has been assessed through the estimation of Dc values in each segment, as indicated in Table 2. The degree of clustering exhibits an inverse relationship with the fractal correlation dimension value. This intricate connection is contingent upon the temporal and spatial aspects of earthquake events. The present investigation focuses on the spatiotemporal occurrences of earthquake series. Therefore, the decreased magnitude of Dc indicates an increased level of event aggregation, while the increased magnitude indicates a decreased level of event clustering. Henceforth, the utilization of the correlation fractal dimension has the potential to provide an estimation of the level of intricacy pertaining to seismotectonic components within a region that experiences active seismic activity (Dasgupta et al., 2000). The temporal fluctuations in the fractal dimension of seismic activity indicate the ongoing transformation of states and the vigour of the system.

4.2 Identifying Ionospheric TEC Values for Seismic Correlation Analysis in North-East India

The data undergoes compilation and processing at the Center for Orbit Determination in Europe (CODE), employing a thin shell model of the Earth's Ionosphere. The assumption made in this context facilitates the computation of the global Total Electron Content (TEC) distribution, denoted as T, using a Spherical Harmonic Expansion formulation as described by Schaer et al. in 1996.

$$\mathbf{T}(\boldsymbol{\alpha},\boldsymbol{v}) = \sum_{\boldsymbol{n=0}}^{\boldsymbol{n(max)}} \sum_{\boldsymbol{m=0}}^{\boldsymbol{n}} \boldsymbol{Inm}\left(\boldsymbol{a_{nm}}\mathbf{cos}(\mathbf{mv}) + \boldsymbol{b_{nm}}\mathbf{sin}(\mathbf{mv})\right) \quad (\mathbf{2})$$

The vertical total electron content (vTEC), denoted as T, has been quantified through the utilization of Equation 2. In this equation, α represents the geocentric latitude of the intersection point between the line receiver-satellite and the ionospheric layer. Furthermore, v corresponds to the Sun-fixed longitude of the ionospheric pierce point, which signifies the disparity between the Earth-fixed longitude and the Sun's longitude. Additionally, n(max) denotes the highest degree of the spherical harmonic expansion, while I_{nm} signifies the normalized associated Legendre functions with a degree of n and an order of m. The coefficients a_{nm} and b_{nm} represent crucial model parameters in this context.

4.2. (a) Analysis of vTEC Anomalies

The daily provision of ionospheric vTEC values is facilitated by NASA through the anonymous ftp server (ftp://cddis.gsfc.nasa.gov). The spatial resolution of the data is 2.5° in latitude and 5° in longitude, while the temporal resolution is 1 hour. The analysis focuses on the temporal fluctuation of Total Electron Content (TEC) at the nearest grid point to the epicentre, utilizing the quartile-based statistical analysis technique. The identification of anomalous Total Electron Content (TEC) behaviour is conducted by comparing it to the past 15-day running median (m) and standard deviation (σ), as described by Liu et al. (2009). The upper and lower quartiles are denoted in equation (3) (82% confidence level).

Upper Bound (UB)= past 15 days running (Median (m) + 1.34 Standard Deviation (σ))

…. **(3)**

Lower Bound (LB) = past 15 days running (Median (m) - 1.34 Standard Deviation (σ))

The occurrences during which vTEC values surpass these predetermined thresholds are identified as anomalous.

4.3. Identifying Atmospheric Anomalies in Air Temperature (AT) and Relative Humidity (RH):

To study the LAIC mechanism, we have also studied the temporal variation of atmospheric air temperature (AT) and relative humidity (RH) at 2m height for duration of one month prior to the earthquakes. To identify any perturbation in these parameters we have constructed upper and lower bounds using hourly mean (μ) and standard deviation (σ) based on past 5 years hourly data. The upper and lower bounds are donated in equation (4) as described by (Orte et al, (2021), Salh et al, (2022) (95% confidence level).

Upper Bound = Past 5 years hourly (Mean (μ) + 2 * Standard Deviation (σ)) ..(4)

Lower Bound = Past 5 years hourly (Mean (μ) - 2 * Standard Deviation (σ))

If the observed parameter falls outside either of these bounds, it will be marked as anomalous. The observed anomalies in the aforementioned parameters play a crucial role in understanding the LAIC mechanism as discussed by earlier workers like Pulinets and Boyarchuk, (2004); Mansouri Daneshvar et al, (2017).

4. 4. Statistical validation of the observed TEC anomaly using ARIMA Model:

The statistical ARIMA model is mainly used for time series forecasting. The working principle of this model is based on the integration of two fundamental methods: Auto Regression (AR) and Moving Average (MA). The ARIMA model stands for Auto-Regressive Integrated Moving Average. This Model consists of 3 parameters:

a. **Auto Regressive Term (p):** Shows an auto regression of a continuously changing variable on its own lagged or prior values.
b. **Non-seasonal Difference (d):** To make the data series stationary we sometimes prefer differencing of the raw data from the previous data point.
c. **Moving Average Term (q):** MA model is applied to the lagged observations, which deals with the dependency b/w the data point and residual error.

To validate those observed ionospheric anomaly using ARIMA model, we have started with the Augmented Dickey Fouler (ADF) test to check the stationarity of the time series data. If the dataset is found to be nonstationary, then we have to compute initial difference (d). The order of d is defined as in equation (5).

$$\Delta Y_t = Y_t \text{ (for d = 0)} \quad (5)$$

$$\Delta Y_t = Y_t - Y_{t-1} \text{ (for d = 1)}$$

Upon achieving stationarity, the seasonality component has been successfully eliminated from the data. The ARIMA model (p, d, and q) was selected using the Box and Jenkins methodology. The determination of the values of p and q can be achieved through the utilization of the partial autocorrelation (PACF) function and autocorrelation (ACF) function, respectively, as outlined in the works of Dutta et al. (2019) and Saqib et al. (2021). The selection of the optimal ARIMA model is determined by evaluating the minimal values of the Akaike Information Criterion (AIC), Bayesian Information Criterion (BIC), and the standard deviation of the parameter. In accordance with the aforementioned criteria, the ARIMA (p, d, q) model under consideration can be mathematically represented as follows:

$$\boldsymbol{Y_t = \alpha_1 Y_{t-1} + \alpha_2 Y_{t-2} + \alpha_3 Y_{t-3\ldots} \alpha_p Y_{t-p} + \varepsilon_t - \theta_1 \varepsilon_{t-1} - \theta_2 \varepsilon_{t-2} - \theta_3 \varepsilon_{t-3\ldots} - \theta_q \varepsilon_{t-q} + \delta} \quad (6)$$

Where, Y_t is a linear combination of previous time series terms, with coefficient α_1, α_2.. and ε_t is random shock. δ is a constant.

5. Results

5.1. Fractal correlation dimension (Dc) value:

The seismic events are graphically represented using Figure 2 and Figure 3, depicting the earthquakes that transpired during the specified timeframe. Additionally, it has been observed

that the (Dc) value exhibits a declining trend within the region. The temporal fluctuations of the Dc value from 2014 to 2021 are depicted in Figure 4, illustrating their relationship to the average time period. The observed variation in Dc values serves as a valuable indicator of the inherent heterogeneity within a given medium. Based on recent findings, it has been noted that the Dc value exhibits variation within the range of 0.742 to 1.496 in the North East region of India. The fractal behaviour of seismicity is contingent upon a multitude of parameters, such as the presence of earthquake location errors, the influence of boundary effects, and the non-uniformity of depth distribution. Based on the findings of (Hirata et al., 1989), it has been observed that the fractal dimension value reaches its maximum at 1.6. This phenomenon has been elucidated through the application of the Griffith energy balance concept. The observed high D_C value, in proximity to the value of two, indicates a reduced level of heterogeneity within the medium, as reported by Tosi et al. in 1998. The observed low values of the fractal correlation dimension indicate a notable concentration of stress, while the high values correspond to the occurrence of smaller earthquakes with minimal stress accumulation. The inverse relationship between the Dc value and clustering is observed, wherein the Dc value exhibits an inverse correlation with the degree of grouping exhibited by a set of events within a specific region (Kagan and Knopoff, 1980; Roy and Mondal, 2009).

5.2. Observed Ionospheric Anomaly in North-East India, April 13, 2016, Mw=6.9:

On April 13th, an event of magnitude Mw 6.9 occurred in Myanmar, at the local time of 13:55 UTC, which was 135 km North-west of Mandalay. The TEC series exhibits estimations of lattice point limits, both upper and lower, that are determined to be in closest proximity to the epicentre. Significant negative anomalies were observed on the 20th, 21st, and 22nd of March, as well as on the 23rd, 26th, and 30th of March, and finally on the 9th of April in the year 2016. The aforementioned time intervals, namely 4, 14, 18, 21, 22, 23, and 24 days were preceding the significant seismic event of considerable magnitude that occurred on April 13, 2016 (Figure 5). The Ap indices and $F_{10.7}$ values are shown in Fig. 5(b) and Fig. 5(c) for the time period

spanning from 17th March to 15th April, 2016 correspondingly, to monitor magnetic storm and solar storm. No significant magnetic storm was recorded during the entire span (Ap index<35). While in case of $F_{10.7}$ index, an increase in solar flux have been observed during the span, indicating moderate ($F_{10.7}$>82) to high solar storm. In-spite of the presence of the solar storm a series of significant decrease in Total Electron Content (TEC) has been observed. Which suggests a potential precursor to an important seismic event in the region? The anomalies observed can plausibly be linked to the seismic event.

5. 3. Observed Ionospheric Anomaly in North-East India, Nov.17. 2017, Mw 6.4:

On November 17, 2017, a significant event of Mw 6.4 occurred at a shallow depth of 10 km closer to Nyingchi City, located in the border region between southwestern China and NE India. The TEC scores, along with their lower and upper limits, were taken into account for the network point in closest proximity to the epicenter. A sequence of notable negative Total Electron Content (TEC) anomalies was detected on the 1st, 5th, 6th, 7th, 9th, 10th, 11th, 12th, and 13th of November preceding the seismic tremor that occurred on November 17, 2017, as depicted in Figure 6 (a). The Ap indices and $F_{10.7}$ variations are depicted in Figure 6(b) and Figure 6(c) respectively, spanning the time period from October 21st to November 19th, 2017. A notable decrease in the Total Electron Content (TEC) measurements was noted on the fourth, fifth, sixth, seventh, eighth, tenth, eleventh, twelfth, and sixteenth days preceding the significant seismic occurrences. However, it is worth mentioning that a comparatively elevated TEC value was observed on the day when the major tremor took place. To rule out any possible contributions from solar terrestrial environment we have also monitored the Ap index and $F_{10.7}$ index. From the above figure (Figure 5(b)) it is observed that, no significant magnetic storm has been reported during the entire span of investigation except from 7th Nov to 10th Nov (Ap index > 35). On the other hand, the variation of F10.7 index shows prominent evidences of the presence of moderate solar storm ($F_{10.7}$>82). This gives us a conclusive evidence in favour of the seismogenic origin of the observed ionospheric anomaly.

5.4. Observed Ionospheric Anomaly in North-East India, April, 28, 2021, Mw 6.0:

A seismic event of significant magnitude Mw 6.1 at a focal depth of 35 km occurred in Dhekiajuli, Assam, India on April 28 UTC. The seismic event reached a maximum intensity of VII on the Modified Mercalli Scale, indicating a classification of "Very strong." A total of six aftershocks have been documented, with the highest magnitude recorded at Mw 4.1. The TEC data for a 45-day period preceding the event was extracted from the grid point closest to the epicenter and subsequently analyzed in relation to the 15-day median, lower bound, and upper bound, as previously described. On the 3rd, 4th, 9th, 10th, 20th, 21st, and 26th of April, a sequence of notable negative anomalies was detected (see Fig. 7a). The seismic event occurred at intervals of 2, 7, 8, 18, 19, 24, and 25 days preceding the occurrence of the mega earthquake. The analysis of the earthquake-induced anomalies was further corroborated by examining the space weather conditions pertaining to the $F_{10.7}$ and AP indices within the timeframe of April 1st to April 30th (as depicted in Figure 7b and 7c). During the aforementioned period, it was noted that there was an absence of geomagnetic storms (with an Ap index below 35) and the solar activity exhibited a state of low intensity, characterized by a tranquil nature (with an $F_{10.7}$ index not exceeding 100).

6. Observed Anomaly in atmospheric air temperature (AT) and relative humidity (ARH):

To demarcate any possible short term perturbations in atmospheric air temperature (AT) and relative humidity (RH), we have analyzed the hourly mean (μ) and standard deviation (μ) of the epicenter for past 5 year prior to the earthquake. We have flagged anomalous behavior based the constructed upper and lower bounds as mentioned in equation (4).

6.1. Observed Atmospheric Anomaly prior to the Mw 6.9 Earthquake:

The hourly varying AT and ARH data sets have been analyzed from 10th March to 19th April, 2016. Anomalous behavior was marked based on the aforementioned method. A series of very prominent temperature rise (AT > Upper Bound) has been observed of the order of 1.5ºC to 4.6 ºC prior to the earthquake (Figure 8(a)). The temperature rise leads to a drop (-ve) in the relative humidity by a significant amount during the same observation period. The diurnal variation of the RH shows prominent -ve anomalies from 6th April to 15th April. The magnitude of the anomaly is of the order of -15 to 21%, as shown in Figure 8(a).

6.2. Observed Atmospheric Anomaly prior to the Mw 6.4 Earthquake:

The temporal variation of AT and RH has been analyzed from 1st Oct to 15th Nov 2017. Anomalous variation in AT is observed not only just prior to the earthquake but also on the day of the event and 2 days after the event. After which the anomaly vanishes. The magnitude of the observed AT anomaly is found to be of the order of ~1.2 ºC to 3.6 ºC. Most prominent anomaly in AT was observed during 19th Oct to 23rd Oct and 16th Nov to 20th Nov as shown in Figure 8(b). Significant increase in air temperature leads to the decrease in relative humidity prior to the earthquake. Prominent –ve anomaly has been observed from 1st Nov to 7th Nov. A sharp drop of ~ -40% is reported within the analyzed time span prior to the earthquake as demarcated in Figure 8(b).

6.3. Observed Atmospheric Anomaly prior to the Mw 6.0 Earthquake:

The hourly varying AT and ARH data sets have been analyzed from 15th March to 10th May, 2021 to identify any short term perturbation prior or during the earthquake. Anomalous behavior was marked based on the aforementioned method. A series of very prominent

temperature rise (AT > Upper Bound) has been observed of the order of 1.5ºC to 2.6 ºC during the span of investigation (Figure 8(c)). Most prominent anomaly was seen from 26th April to 2nd May, i.e. 2 days prior to the earthquake to 4 days after the event. The temperature rise leads to a drop (-ve) in the relative humidity by a significant amount during the same observation period. The diurnal variation of the RH shows prominent -ve anomalies from 20th April to 2nd May. The magnitude of the anomaly is of the order of -10 to 31%, as shown in Figure 8(c).

7. Statistical Validation of the observed Ionospheric Anomaly using ARIMA Model:

To validate the observed anomalous behavior of Total Electron Content (TEC) preceding these earthquakes, a statistical Autoregressive Integrated Moving Average (ARIMA) model is employed. To effectively employ the ARIMA model, it is imperative to commence by conducting an Augmented Dickey Fouler (ADF) test and calculating the running average across the dataset. This is done to ascertain the stationarity of the dataset. Upon careful examination of the outcomes derived from the aforementioned procedure, we have conducted a first order difference (d=1) (equation 5) in order to render the data stationary, as indicated by the test statistics, critical value, and p-value (<0.05).

$$\Delta Y_t = Y_t - Y_{(t-1)} \quad \textbf{(for d=1)} \qquad \textbf{(see Eq 5)}$$

In order to select the appropriate ARIMA model (p, d, q) using the Box and Jenkins method, it is customary to derive the value of p from the partial autocorrelation (PACF) function, while the value of q is determined from the autocorrelation (ACF) function (Saqib et al., 2021). The selection of the optimal ARIMA model is contingent upon several factors, including the attainment of the minimum standard deviation, as well as the evaluation of the Akaike Information Criterion (AIC), Schwarz Information Criterion (SIC), and Bayesian Information Criterion (BIC). Upon selecting the appropriate ARIMA model derived from our training dataset, we proceeded to predict the Total Electron Content (TEC) values during the occurrence

of anomalous days. Given that the model in question is of a statistical nature, it is imperative to establish an error bound to assess the precision of the projected Total Electron Content (TEC) value as demonstrated in Equation (7).

Upper Error Bound= forecasted value + 1.34* standard deviation **(7)**

Lower Error Bound= forecasted value - 1.34* standard deviation

It has been clearly observed a significant reduction in the actual TEC values on those anomalous days in comparison with the forecasted TEC values.

7.1. Statistical analysis of TEC data for the earthquake on 13th April 2016, Mw 6.9:

The identification of anomalies is conducted by analyzing a 15-day running median of the upper and lower bounds, which represent the median value plus or minus 1.34 times the standard deviation. The most notable anomaly is observed on the 20th, 21st, 22nd, 23rd, 26th, and 30th of March in the year 2016, as depicted in Figure 5(a). Based on the results of the Augmented Dickey-Fuller (ADF) test, it has been determined that the observed data exhibits non-stationary characteristics. In order to achieve stationarity, the initial differentiation (d=1) has been applied to the dataset. The null hypothesis was disregarded through the examination of the critical values of the test statistics and the p-value. Subsequently, in order to ascertain the appropriate selection of p and q, we have generated a graphical representation of the Partial Autocorrelation Function (PACF) and Autocorrelation Function (ACF) of the given dataset. The observed oscillatory characteristics of the autocorrelation function (ACF) suggest the potential existence of periodic patterns or seasonality within the dataset. Following the elimination of seasonal patterns from the data, we have identified and selected the suitable ARIMA model in accordance with the aforementioned methodologies.

Upon selecting the suitable ARIMA model through the aforementioned approach, we have employed said model to project forthcoming TEC values on the previous atypical days, to

authenticate the source of the negative anomaly as depicted in Figure 9. Upon finalizing the input model parameter, a day without any anomalies has been selected to assess the forecasting accuracy of the model. Upon conducting tests to determine the model's accuracy, we identified a specific day with anomalous behavior. This day has been selected as the basis for forecasting the Total Electron Content (TEC) variation. Consequently, we have generated forecasts for the TEC values specifically for this anomalous day. Given the nature of this statistical model, it is imperative to acknowledge the inclusion of both an upper and lower error bound in relation to the projected forecast. In the event that the TEC value deviates below or above this threshold, it indicates compelling evidence in favor of the TEC anomaly occurring on that particular day. Observations suggest that the recorded Total Electron Content (TEC) values exhibit a notable discrepancy compared to the previously predicted values during anomalous periods.

7.2. Statistical analyses of TEC data for the earthquake on 17th November, 2017, Mw 6.4:

A series of negative ionospheric anomalies was observed before this earthquake as shown in Figure 6(a). To validate this result statistically, we have employed our chosen ARIMA model (p, d, q) using ACF and PACF plots to forecast TEC values for a non-anomalous day. This allows us to assess the accuracy of our forecasting. Subsequently, we have projected the Total Electron Content (TEC) values for the aforementioned days exhibiting anomalies. Given the statistical nature of the model being discussed, it is important to note that an upper and lower error bound has been included in the forecast. These bounds are determined by forecasted values ±1.34 times the standard deviation. In the event that the observed Total Electron Content (TEC) value descends beneath this threshold, we can ascertain compelling evidence indicating the presence of a negative TEC anomaly on that particular day. Based on the analyzed data, it has been noted that the observed Total Electron Content (TEC) values are significantly lower than anticipated. The statistical ARIMA model was utilized to observe the anomalous behavior of TEC on the 1st, 5th, 6th, 7th, 9th, 10th, 11th, 12th, and 13th of November, 2017, as depicted

in Figure 10.

7.3. Statistical analysis of TEC data for the earthquake on 28th April, 2021, Mw 6.0:

The ionospheric perturbation linked to the Assam earthquake on April 28th, 2021 has been thoroughly analyzed using past 15-days running median and standard deviation. A series of –ve TEC anomaly has been observed on the 3rd, 4th, 9th, 10th, 20th, 21st, and 26th of April prior to the earthquake. The temporal variation of negative anomalies was detected in Figure 7(a). To validate these observed anomalies statistically, we have chosen appropriate ARIMA model based on the PACF and ACF plots in accordance with least AIC value. After selecting the appropriate model parameters (p, d, q) we forecasted TEC values for those anomalous days. Given the nature of our analysis as a statistical model, it is imperative to acknowledge the inclusion of both an upper and lower error bound alongside the projected forecast. In the event the observed Total Electron Content (TEC) value descends beneath this threshold, it would indicate compelling evidence in favor of a negative TEC anomaly occurring on that particular day. Based on the analyzed data, it has been noted that the recorded Total Electron Content (TEC) values are significantly lower than the expected values as shown in Figure 11. Furthermore, anomalous TEC patterns were detected on the following dates: 3rd, 4th, 9th, 10th, 20th, 21st, and 26th of April.

8. Discussions

The tectonic configuration of North-East India is characterized by a multitude of fractures and tectonic deviations. The continuous movement of tectonic plates along the subduction zone in this area serves as a reliable indicator of the prevailing tectonic activity in this particular region. The region holds significant importance in the field of earthquake study as it experiences notable earth plate readjustments.

Our observations indicate the occurrence of multiple seismic events with significant magnitudes (Mw ≥ 6) in this particular region. Notable examples include an earthquake with a

magnitude of 6.9 on April 13, 2016, another with a magnitude of 6.4 on November 17, 2017, and yet another with a magnitude of 6.0 on April 24, 2021 (Table 2). The selected earthquakes for analysis consist of a cluster of two closely situated events, while the third event is noticeably distant from the others. In this analysis, we shall examine the seismic data catalogues spanning the temporal range of 2014 to 2021. Based on the recent study, the depiction of the temporal evolution of Dc (fractal correlation dimension) can be observed in Figure 4. It is evident that the value of Dc exhibits fluctuations over the course of the specified time period. Furthermore, the observed phenomenon could potentially be attributed to the relatively short time span between the successive occurrences of numerous earthquakes, resulting in heightened clustering within a specific region. Alternatively, it could be a consequence of prolonged aftershocks preceding the onset of significant main shocks of considerable magnitude (Kagan et al., 1991; Helmstetter et al., 2005). Observing the heightened concentration of intermediate-size events, it is evident that the fractal correlation dimension value exhibits a decline preceding a significant earthquake. The temporal observations indicate a discernible decrease in the Dc value throughout the intervals encompassing December 27, 2014 to August 12, 2015, July 21, 2017 to January 18, 2018, and 24.07.2020 to 08.11.2020. Based on the observed lower Dc value, there is a notable indication of heightened scale invariance clustering within the region. This phenomenon suggests an increased likelihood of a significant earthquake occurring in the near future.

The Ionospheric Total Electron Content (TEC) anomaly is a complex spatiotemporal occurrence which is linked to the Fractal correlation dimension value. It is intricately linked to the micro pulsations that transpire between the Earth's surface and the ionosphere medium situated above it. In our comprehensive analysis, we have diligently examined the TEC (Total Electron Content) data spanning a period of 45 days preceding each projected seismic event. Through our meticulous observations, we have successfully identified the anticipated seismic signature for three notable and impactful earthquakes. As the ionosphere is very sensitive to

solar and magnetic storm, thus to rule out any possible contribution due to these we have kept a close eye on these, parameters using $F_{10.7}$ index and Ap index. During severe geomagnetic storms, its variation typically reaches 100. Solar flux ($F_{10.7}$) index varies between 70 and 120. Where 700 is marked as quiet, and the $F_{10.7}$>120 is flagged as high solar storm.

The ionosphere data has been subjected to a comparative analysis with the Fractal correlation dimension, as both parameters exhibit variations in relation to changes in time and spatial distribution. The investigation of Total Electron Content (TEC) fluctuations in relation to low Direct Current (Dc) values reveals the presence of elevated stress levels accompanied by intensified clustering patterns, suggesting a heightened likelihood of a seismic event of significant magnitude. A recent study pertaining to the seismic event that transpired on April 13, 2016, provides corroborative evidence suggesting that earthquakes occurring at greater depths exhibit a higher degree of efficacy in stress dissipation when compared to a shallower earthquake transpiring on November 17, 2017. The potential cause for the increased emission of Radon gas and the occurrence of a TEC anomaly over a larger geographical area during the earthquake on April 13, 2016 (at a depth of 136 km), as opposed to the earthquake on November 17, 2017 (at a depth of 8 km), is under consideration. Furthermore, based on the correlation observed between the aforementioned seismic events, it can be deduced that an increase in the negative deviation of Total Electron Content (TEC) values corresponds to a greater magnitude of the forthcoming earthquake. Furthermore, in relation to the seismic event that occurred on November 17, 2017, it is observed that the existing Total Electron Content (TEC) fluctuations exhibit a limited number of negative deviations when compared to the average TEC flux value. Additionally, the magnitude of the earthquake recorded was Mw- 6.4. In relation to the earthquake that occurred on April 13, 2016, it has been observed that the current Total Electron Content (TEC) variation exhibits a notable negative deviation. This deviation signifies a higher value compared to the average TEC flux. The earthquake itself has been measured to have a magnitude of Mw- 6.9 on the Richter scale. The observed low Dc value may potentially be

attributed to heightened internal clustering phenomena within the Earth, consequently leading to indirect repercussions on the ionosphere. These repercussions manifest as alterations in electronic pulsations, thereby contributing to the observed changes. Based on observations, it has been determined that the Dc value exhibits a decrease either prior to or during a prolonged period leading up to a seismic event of significant magnitude. In contrast, the TEC value demonstrates variability in the days preceding the occurrence of a strong event. By employing the integration of these two methodologies, a more robust framework has been established to anticipate the imminent occurrence of a seismic event of significant magnitude.

The major objective of this paper is to identify any short-term perturbation in atmospheric air temperature (AT), relative humidity (RH), ionospheric TEC and Dc fractal analysis before the occurrence of a significant earthquake with a magnitude Mw $\geq$ 6. Further, a new attempt was made to validate this observed ionospheric anomaly statistically using ARIMA model. Here, we have carried out a multi-parametric earthquake precursory studies for 3 major earthquakes, which has occurred in different area and time. Apart from the Dc fractal analysis and ionospheric perturbations, very prominent anomalies are observed in air temperature (AT) and relative humidity (RH). A sharp increase in AT ~ 1.5- 4.6 ºC is observed before the Mw 6.9 earthquake, which eventually gives rise to a drop of RH by ~20%. In the case of the Mw 6.4 event, the observed anomaly (+ve) in AT is ~ 1.2º-3.6 ºC, whereas the observed RH anomaly is ~ -40%. Focusing on the Mw 6.0 event shows a prominent temperature rise in AT ~ 1.5º - 2.6ºC and a sharp drop in relative humidity ~ -10 to -31% prior to the earthquake.

In our diligent pursuit, we have endeavoured to ascertain the potential whereabouts of forthcoming seismic activity by analyzing the distribution of past earthquake events, as depicted in Figure 2 and Figure 3. The seismicity patterns in these two figures illustrate the spatial distribution of earthquake events leading up to a significant seismic event, coinciding with a gradual decrease in the Dc value. Figure 2 depicts the utilization of blocks A and B to represent the highest concentration of events within a specific region from December 27, 2014,

to August 12, 2015. In block A, we observe two robust seismic events characterized by their distinct focal mechanism distribution. These seismic occurrences are constraints within the Eastern Boundary zone, which is known for its seismic activity. The seismic behaviour of the EBZ exhibits a predominant transformation from strike-slip faulting to dip-slip faulting as it progresses towards the southern orientation. Based on our observations within the exact figure, it is evident that a series of minor seismic occurrences tend to congregate as preliminary tremors within a concentrated area in block B. This clustering phenomenon potentially signifies the likelihood of an impending seismic event of significant magnitude. Based on our observations in (Fig.3), an essential seismic event has been detected in the vicinity of block B, exhibiting an elongated duration. A Sequence of foreshocks is observed in Fig. 2, block B, before the occurrence of the intense earthquake event depicted in Fig. 3. At long last, can witness a significant multitude of occurrences within block C, potentially serving as an indication of an imminent seismic event of considerable magnitude in the EBZ region. Based on our analysis, it indicates that this particular region exhibits a significant level of tectonic activity.

9. Conclusions

The primary objective of this paper is to investigate the short-term perturbation in atmospheric air temperature (AT), relative humidity (RH), ionospheric TEC and Dc fractal analysis before the occurrence of a significant earthquake with a magnitude Mw ≥ 6. Further, a novel approach helps to validate this observed ionospheric anomaly statistically using the ARIMA model. The analysis of spatio-temporal Total Electron Content (TEC) variation allows for considering the potential earthquake's magnitude, location, and timing, which are fundamental factors in seismic forecasting. Similarly, fractal correlation measurement, derived from seismic data indices, presents a viable approach for long-term predictive computations about a particular region. By utilizing these essential systems, we can accurately assess the likelihood of an

earthquake occurrence. Anticipating seismic tremors will no longer be a 'Mind-boggling' phenomenon. Our current study, has determined that the EBZ region exhibits the highest level of seismic activity within North East India. This multi-parametric earthquake precursory study will provide some beneficial insights for future researchers to understand the lithosphere atmosphere ionosphere coupling (LAIC) mechanism.

Acknowledgments

The authors are gratefully acknowledging Ministry of Earth Sciences, Govt. of India for partly sponsoring this work (No. MOES/P.O. (Seismo)/1(364)/2019).

References

Chen, W. P., Molnar, P., 1990. Source parameters of earthquakes beneath the Shillong Plateau and the Indo burman ranges. J. Geophys. Res. 95, 12527–12552.

Dasgupta, S., Pande, P., Ganguly, D., Iqbal, Z., Sanyal, K., Venaktraman, N. V., Dasgupta, S., Sural, B., Harendranath, L., Mazumadar, S., Sanyal, S., Roy, A., Das, L. K., Misra, P. S., Gupta, H., 2000. Seismotectonic Atlas of India and its Environs. Geological Survey of India, Calcutta. P. 87.

Davies, K., Baker, D. M., 1965. Ionosphere effects Observed around Time of Alaskan Earthquake of March 28, 1964. J. Geophy. Res. 70, 2251-2253.

Depueva, A., 2012. Peculiarities of low-latitude and equatorial ionosphere prior to strong earthquakes. Geom. Nat. Hazards Risk. 3, 207-224.

Dogan, U., Ergintav, S., Skone, S., Arslan, N., Oz, D., 2011. Monitoring of the ionosphere TEC variations during the 17th August 1999 Izmit earthquake using GPS data. Earth Planets Space 63, 1183-1192.

Dutta. B., Mondal. I., Champatiray, P. K., Agrawal. M., 2019. Forecasting of Global Ionospheric Perturbation Using GIM and ARIMA as a Precursor of Earthquake", Earth Doc, 81st EAGE Annual Conference and Exhibition, London, UK. DOI:10.3997/2214-4609.201901068.

Fitch, T. J., 1970. Earthquake mechanism in the Himalayan, Burmese and Andaman region and continental tectonics in Central Asia. J. Geophysics Res. 75, 2699-2709.

Freund, F. T., Kulahci, I. G., Cyr, G., Ling, J., Winnick, M., Tregloan-Reed, J., Freund, M. M., 2009. Air ionization at rock surfaces and pre-earthquake signals. J. Atmos. Solar-

Terrestrial Phys. 71, 1824-1834. DOI: 10.1016/ j.jastp.2009.07.013.

Freund, F., 2010. Pre-earthquake signals: Underlying physical processes. Journal of Asian Earth Science, 41, 383-400.

Freund, F., 2013. Earthquake Forewarning- A Multidisciplinary Challenge from the Ground up to Space. Acta Geophysica 61(4), 775-807. DOI: 10.2478/s11600-013-0130-4.

Freund, F., Ouillon, G., Scoville, J., Sornette, D., 2017. Earthquake precursors in light of the peroxy defect theory: Critical review of systematic observations. European Physical Journal. 1, 1711-01780.

Grassberger, P., Procaccia, I., 1983. Measuring the strangeness of strange attractors. Physica. 9, 189–208.

Heki, K., 2011. Ionospheric electron enhancement preceding the 2011 Tohoku-Oki earthquake. Geophys. Res. Lett. 38, L17312.doi.org/10.1029/2011GL047908.

Heki, K., Enomoto, Y., 2013. Preseismic ionospheric electron enhancements revisited. J. Geophys. Res. Space Phys. 118, 6618-6626.

Helmstetter, A., Kagan, Y. Y., Jackson, D. D., 2005. Importance of small earthquakes for stress transfers and earthquake triggering. J. Geophys. Res. 110, 1-13. B05S08. DOI: 10.1029/2004JB003286.

Hirata, T., 1989. A correlation between the b value and the fractal dimension of earthquakes. J. Geophys. Res. 94, 7507– 7514.

Hoppel, W. A., Anderson, R. V., and J. C., 1986. Atmospheric electricity in the planetary boundary layer in The Earth's Electrical Environment. Natural Academic Press, Washington, D. C. 149–165.

Kagan, Y. Y., 2007. Earthquake spatial distribution: the correlation dimension. Geophys. J. Int. 168, 1175–1194.

Kagan, Y. Y, Knopoff, L, 1980. Spatial distribution of earthquakes: The two point correlation function. Geophys. J. R. Astr. Soc. 62, 303–320.

Kayal, J. R., 1987. Microseismicity and source mechanism study: Shillong Plateau, North East India. Bull. Seismol. Soc. Am. 77(1), 184–194.

Klotz, S., Johnson, N. L., 1983. Encyclopedia of statistical sciences. A Wiley Interscience Publication, John Wiley and Sons, New York. 1-9.

Kagan, Y. Y., 1991. Fractal dimension of brittle fracture, J. Nonlinear Sci1. 1–16.

Le Dain, A. Y., Tapponnier, P., Molnar, P., 1984. Active faulting and tectonics of Burma and surrounding regions. J. Geophys. Res. 89, 453–472.

Leonard, R. S., Barnes. R. A., 1965. Observation of ionospheric disturbances following Alaska earthquake. J. Geophys. Res. 70, 1250-1253.

Liperovsky, V. A., Pokhotelov, O. A., Liperovskaya, E. V., Parrot, M., Meister, C. V., Alimov, O. A., 2000. Modification of sporadic E-layers caused by seismic activity. Surv. Geophys. 21, 449_486.

Liu, J. Y., Chuo, Y. J., Shan, S. J., Tsai, Y. B., Chen, Y. I., Pulinets, S. A., Yu, S. B., 2004. Pre-earthquake ionospheric anomalies registered by continuous GPS TEC measurements. Ann. Geophys. 22, 1585-1593.

Liu, J. Y., Chen, Y. I., Chuo ,Y. J., and Chen ,C. S., 2006. A statistical investigation of pre-earthquake ionospheric anomaly, Journal of Geophysical Research. 111, A05304, http://dx.doi.org/10.1029/2005JA011333 .

Liu, J. Y., Chen, Y. I., Chen, C. H., Liu, C. Y. , Chen, C.Y., Nishihashi, M., Li, J. Z., Xia, Y. Q., Oyama, K. I., Hattori, K. , Lin, C. H., 2009. Seismo-ionospheric GPS total electron content anomalies observed before the 12 May 2008 M (w) 7.9 Wenchuan earthquake. J. Geophys. Res. doi: 10.1029/2008JA013698.

Liu, J. Y., Chen, C.H., Chen, Y.I., Yang, W.H., Oyama, K.I., Kuo, K. W., 2010. A Statistical Study Of Ionospheric Earthquake Precursors Monitored By Using Equatorial Ionization Anomaly Of GPS TEC In Taiwan During 2001–2007, Journal Of Asian Earth Sciences. 39, 76–80.

Mansouri Daneshvar, M.R., Freund, F.T., 2017. Remote Sensing of Atmospheric and Ionospheric Signals Prior to the Mw 8.3 Illapel Earthquake, Chile 2015, the Chile- 2015 (Illapel) Earthquake and Tsunami. 11–45.

Mitchell, A. H. G., 1981. Phanerozoic plate boundaries in mainland SE Asia, the Himalaya and Tibet, J. Geol. Soc. Lond. 138, 109–122.

Mitchell, A. H. G., McKerrow, W. S., 1975. Analoguous evolution of the Burma orogen and the Scottish Caledonides. Geol. Soc. Am. Bull. 86, 305–315.

Nandy, D. R., 2001. Geodynamics of North-eastern India and Adjoining Region. ABC Publ. Kolkata, India. 209.

Ni, J., York, J. E., 1978. Late Cenozoic tectonics of the Tibetan plateau. J. Geophysics. Res. 83, 5377-5384.

Orte, F., Lusi, A., Carmona, F., D'Elia, R., Farami˜n´an, A., Wolfram, E., 2021. Comparison of NASA-POWER Solar Radiation Data with Ground-Based Measurements in the South of South America, 2021 XIX Workshop on Information Processing and Control (RPIC). 1–4.

Otsuka, Y., Kotake, N., Tsugawa, T., Shiokawa, K., Ogawa, T., Effendy, Saito, S., Kawamura, M., Maruyama, T., Hemmakorn, N., Komolmis, T., 2006. GPS detection of total electron content variations over Indonesia and Thailand following the26 December 2004 earthquake. Earth Planets Space. 58, 159-165.

Parrot, M., Achache, J., Berthelier J. J., Blanc, E., Deschamps, A., Lefeuvre, F., Menvielle, M., Plantet, J. L., Tarits, P., Villain, J. P., (1993) High-frequency seismo-electromagnetic effects. Phys. Earth Planet Inter. 77, 65-83.

Pundhir, D., Singh, B., Singh, O. P., 2014. Anomalous TEC variations associated with the strong Pakistan_Iran border region earthquake of 16 April 2013 at a low latitude station Agra, India. Adv. Space Res. 53, 226_232.

Pulinets, S. A., 2004. Ionospheric precursors of earthquakes, Recent advances in theory and practical applications. TAO. 15(3), 413-435.

Pulinets, S. A. and K. Boyarchuk, 2004. Ionospheric Precursors of Earthquakes. Springer-Verlag Publication. ISBN 3540208399, Berlin Heidelberg, Germany.

Pulinets, S. A., Boyarchuk, K. A., Hegai, V. V., Karelin, A. V., 2002. Conception and model of

seismo-ionosphere-magnetosphere coupling. In: Hayakawa, M., Molchanov, O. A. (Eds.), seismo-electromagnetics: Lithosphere-atmosphere ionosphere Coupling Terra. Scientific Publishing Co Tokyo. 353-361.

Roy, P. N. S., Ram, A., 2006. A correlation Integral approach to the study of 26 January 2001 Bhuj earthquake, Gujarat, India. J. Geodyn. 41(4), 385–399.

Roy, P. N. S., Gupta, D. K., 2015. Fractal analyser: A MATLAB application for Multifractal Seismicity Analysis. Seismological Research Letters. 86(5), 1-8. DOI: 10.1785/0220150013.

Roy, P. N. S., Mondal, S. K., 2009. Fractal nature of earthquake occurrence in northwest Himalayan region. J. Indian Geophys. Union. 13(2), 63–68.

Salh, H., Muhammad, A., Ghafar, M. M., Külahcı, F., 2022. Potential utilization of air temperature, total electron content, and air relative humidity as possible earthquake precursors: A case study of Mexico M7.4 earthquake, Journal of Atmospheric and Solar-Terrestrial Physics. 237. 105927 https://doi.org/10.1016/j.jastp.2022.105927.

Saquib, M., Senturk, E., Sahu, S. A., Adil, M. A., 2021. Ionospheric anomalies detection using autoregressive integrated moving average (ARIMA) model as an earthquake precursor. Acta Geophysica, Atmospheric and Space Sciences. 69, 1493–1507. doi:10.1007/s11600-021-00616-3.

Schaer, S., Beutler, G., Rothacher , M., Springer, T. A., 1996a Daily Global Ionosphere Maps Based on GPS Carrier Phase Data Routinely Produced by the CODE Analysis Center, In: Proceedings of the IGS AC Workshop, Silver Spring. MD, US. 19–21,181–192.

Sharma, K., Dabas, R. S., Sarkar, S. K., Das, R. M., Ravindran, S., and Gwal, K. 2010. Anomalous Enhancement of Ionospheric F2 Layer Critical Frequency and Total Electron Content over Low Latitudes before Three Recent Major Earthquakes In China. Journal of Geophysical Research 115, A11313, Http://Dx.Doi.Org/10.1029/2009ja014842.

Silina, A. S., Liperovskaya, E. V., Liperovsky, V. A., Meister, C. V., 2001. Ionospheric phenomena before strong earthquakes. Nat Hazards Earth Syst. Sci. 1, 113_118.

Singh, B., Singh, O. P., 2007. Simultaneous ionospheric E- and F-layer perturbations caused by some major earthquakes in India. Ann. Geophys. Italy. 50, 111-122.

Tosi, P., 1998. Seismogenic structure behaviour revealed by spatial clustering of seismicity in the Umbaria-Marche region (Central Italy). Ann. Geofis. 41(2), 215–224.

Thingbaijam, K. K. S., Nath, S. K.,Yadav, A., Raj, A., Walling, M. Y., Mohanty, W. K., 2007. Recent seismicity in Northeast India and its adjoining region. J. Seismol. 12, 107-123.

Turcotte, D. L., 1986. A fractal model for crustal deformation, Tectonophysics. 132, 261–269.

Venkatanathan, N., Kaarthick, B., 2013. Outgoing Long Wave Radiation Anomalies Associated with Earthquakes of Neighboring Region of India – A Case Study on Earthquakes (Mw – 6.0) during the Period of January 2012 – November 2012. Int. J. of Earth Sci. and Engg. 6.2, 1750 – 1756.

Verma, R. K., Mukhopadhyay, M., Ahluwalia, M. S., 1976. Seismicity, Gravity and Tectonics of North east India and Northern Burma. Bull. Seism. Soc. Am. 66, 1683-1694.

Xu, T., Hu, Y. L., Wang, F. F., Chen, Z., and Wu, J. 2015. Is There Any Difference In Local Time Variation In Ionospheric F2-Layer Disturbances Between Earthquake-Induced And Q-Disturbance Events?. Ann. Geophys., 33, 687–695.

Zhou, Y., Wu, Y., Qiao, X., Zhang, X., 2009. Ionospheric anomalies detected by ground-based GPS before the Mw 7.9 Wenchuan earthquake of May 12, 2008, China. J. Atmos. Solar Terres. Phys. 71, 959-966.

Figure Captions.

Fig. 1. The study area North East India which constitute of latitude 22° N to 31° N and longitude 92°E to 101°E. All faults and thrust lines and three strong magnitude earthquake location Mb ≥ 6 has been plotted. Here following abbreviation has been used for MCT-Main Central Thrust. MBT-Main Boundary Thrust, T-Thrust, F-Fault.

Fig. 2. Depicts all earthquake events in Block A and Block B that occurred during the time period of low Dc value along with following two strong events focal mechanisms, which occurred after the time period of low Dc.

Fig. 3. Depicts all earthquake events in Block C that occurred during the time period of low Dc value along with following strong event focal mechanism, which occurred after the time period of low Dc. Following abbreviation has been used EHZ-Eastern Himalayan Zone, MBZ-Mishmi Boundary Zone, and EBZ-Eastern Boundary Zone.

Fig. 4. Dc versus Mean time (in month) has been plotted, where strong earthquake occurrence is indicated after the time period of low Dc value.

Fig. 5 (a). Temporal variation of TEC along with lower, upper abound with prominent anomaly as observed during, before Myanmar Earthquake of 13th April, 2016 (b) Ap Index and (c) F10.7 scale covering the event (17th March to 15th April 2016). (Data Used: GNSS (IGS) derived TEC value, (NASA).

Fig. 6 (a). Temporal variation of TEC along with lower, upper abound with prominent anomaly as observed during, before Shi Yomi Earthquake of 17th November, 2017 (b) Ap Index and (c) F10.7 scale covering the event (21st October to19th November 2017). (Data Used: GNSS (IGS) derived TEC value, (NASA))

Fig. 7 (a). Temporal variation of TEC along with lower, upper abound with prominent anomaly as observed during, before Assam Earthquake of 28th April, 2021 (b) Ap Index and (c) F10.7 scale

covering the event (1st April to 30th April 2021). (Data Used: GNSS (IGS) derived TEC value, (NASA))

Fig. 8(a). Temporal variation of the observed anomaly in atmospheric Air Temperature and Relative Humidity at 2m height prior to the Myanmar earthquake (Mw 6.9) (b) Temporal variation of the observed anomaly in atmospheric Air Temperature and Relative Humidity at 2m height prior to the Shi Yomi earthquake (Mw 6.4) (c) Temporal variation of the observed anomaly in atmospheric Air Temperature and Relative Humidity at 2m height prior to the Assam earthquake (Mw 6.0)

Fig.9. Identification of anomalous Behaviour of TEC using statistical ARIMA model for Mawlaik Earthquake, Myanmar (Mw 6.9).

Fig. 10. Identification of anomalous Behaviour of TEC using statistical ARIMA model for Shi Yomi Earthquake (Mw 6.4).

Fig. 11. Identification of anomalous Behaviour of TEC using statistical ARIMA model for Assam Earthquake (Mw 6.0).

Fig. 1

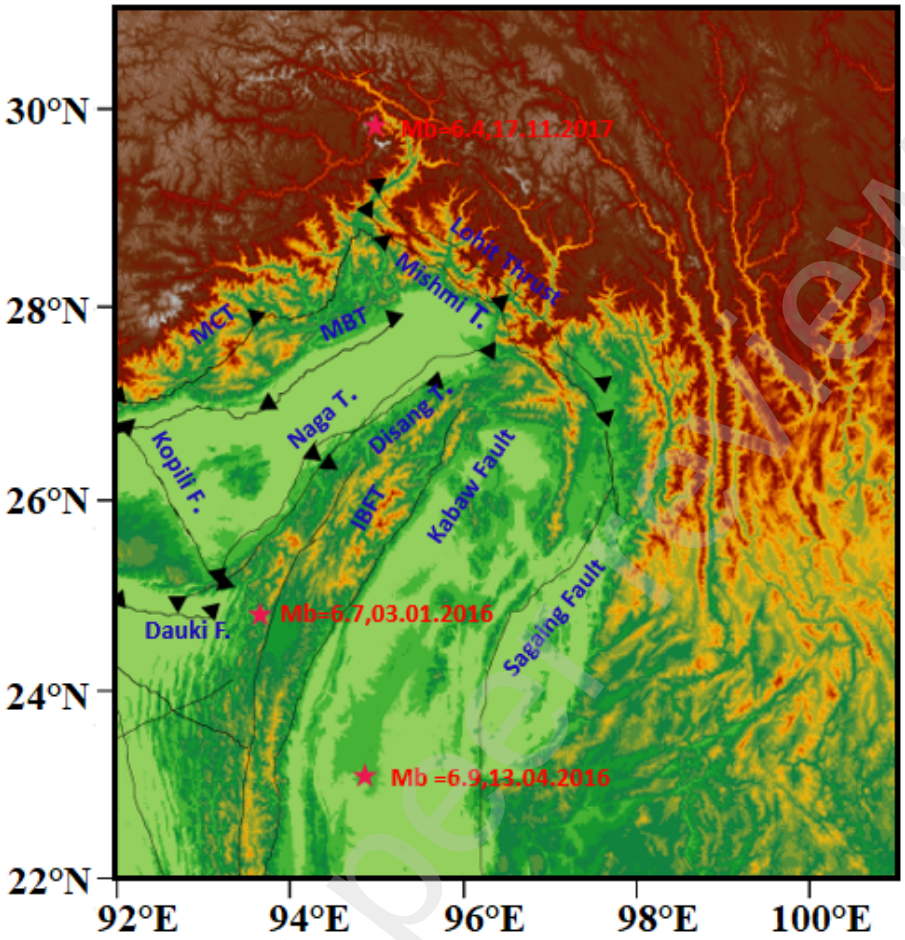

Fig. 2

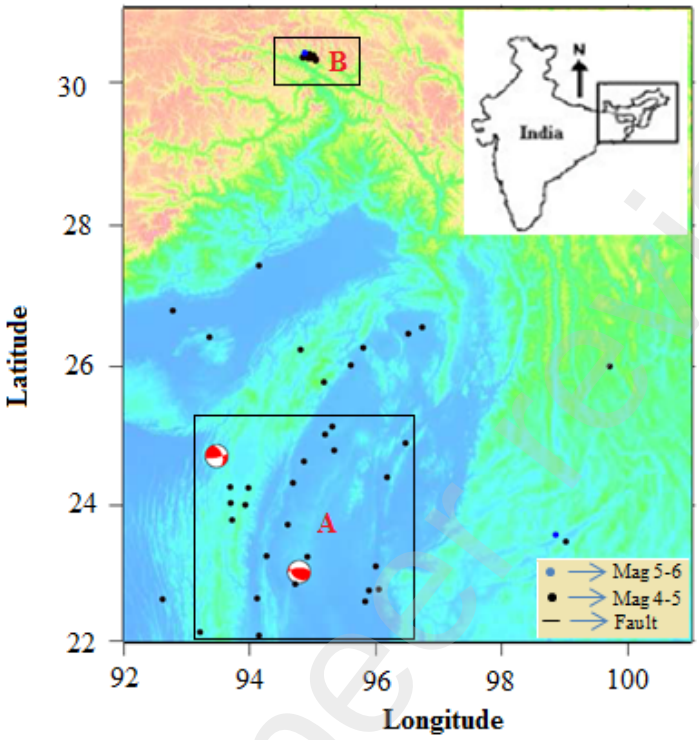

Fig. 3

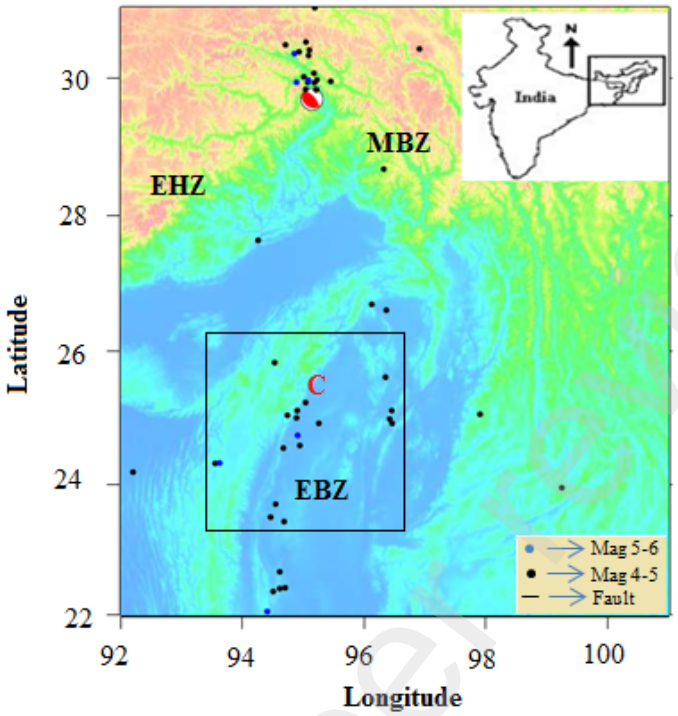

Fig. 4

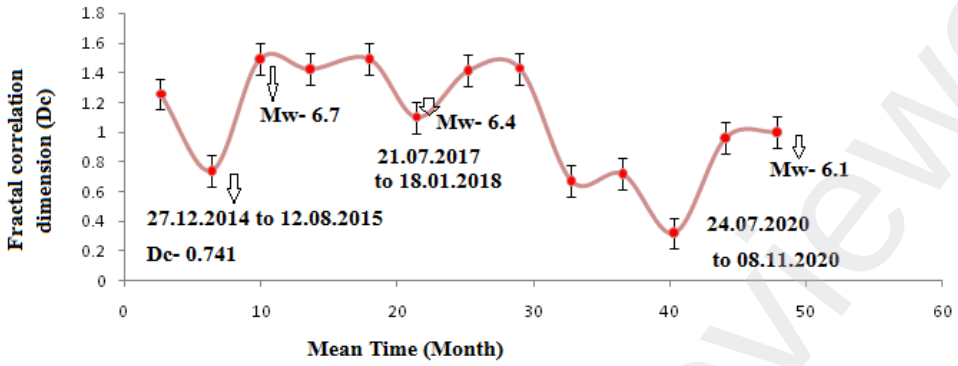

Fig. 5a

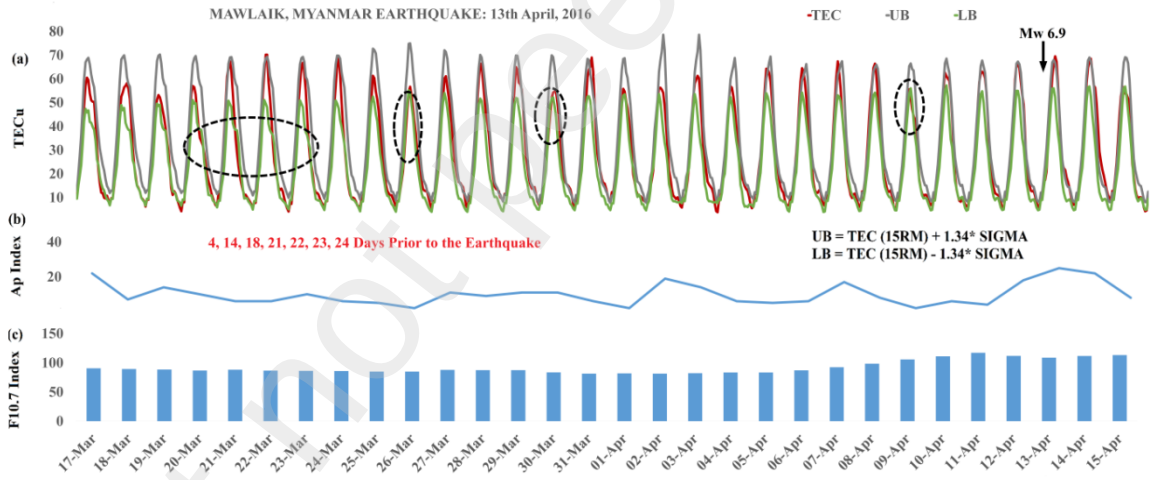

Fig. 6a

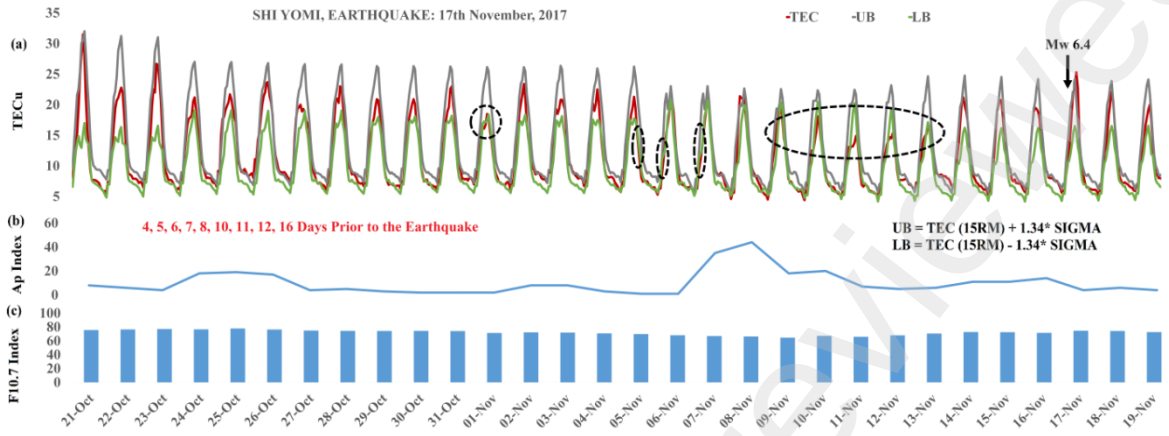

Fig. 7a

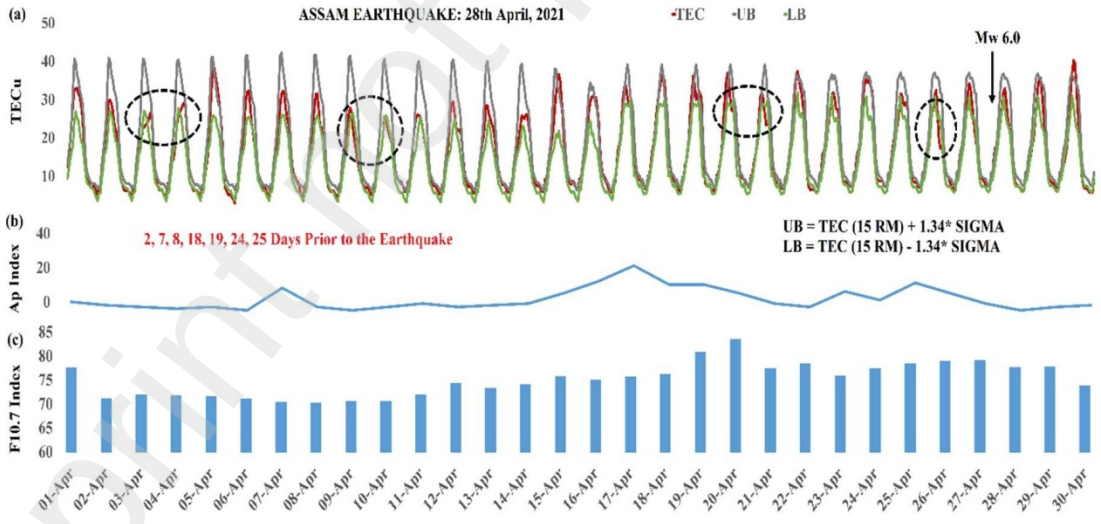

Fig. 8(a), (b), (c)

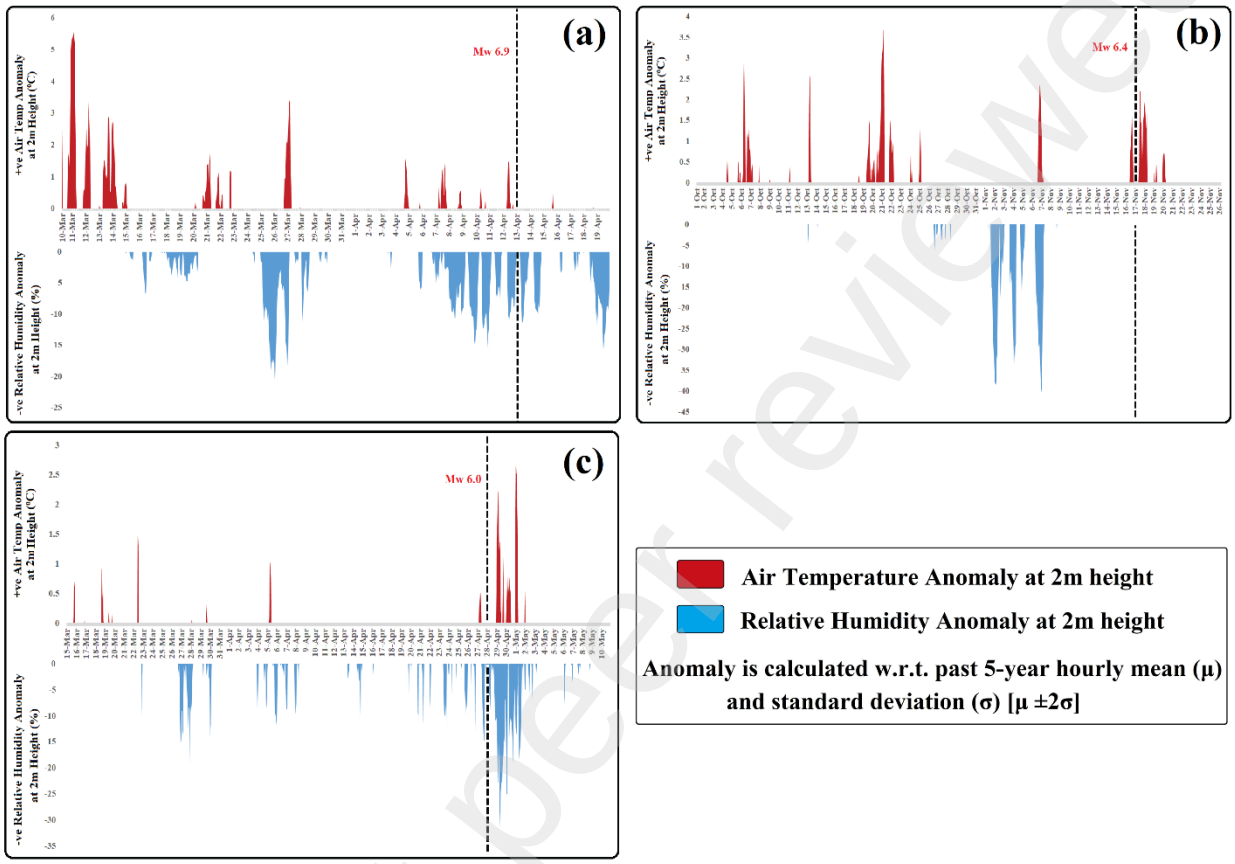

Figure 09

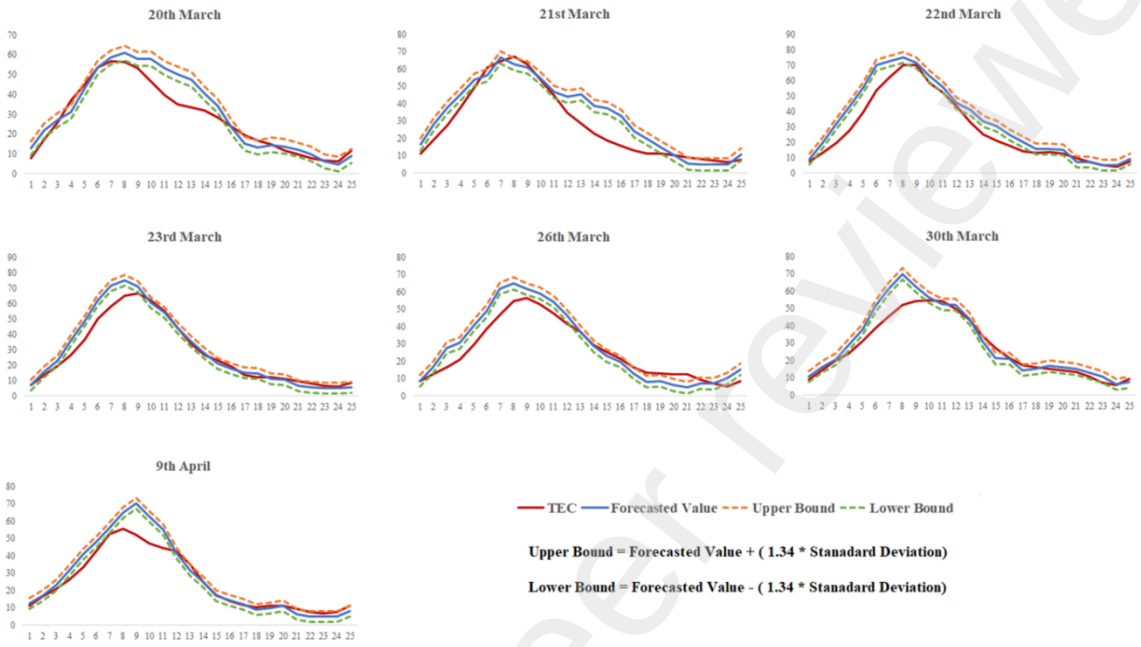

Fig 10.

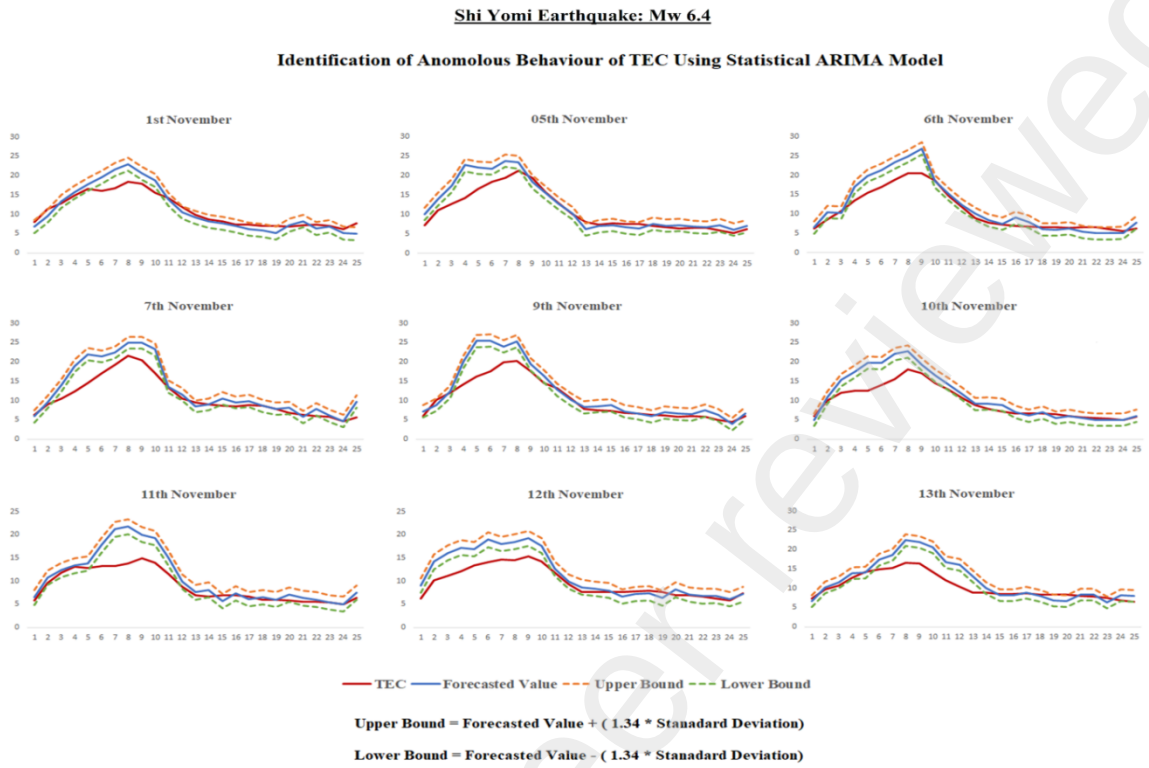

Fig. 11.

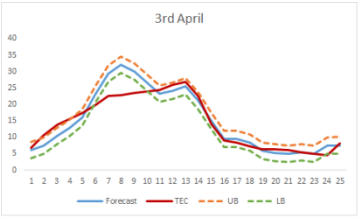

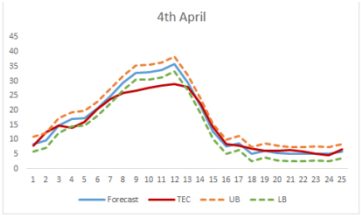

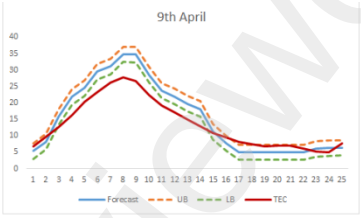

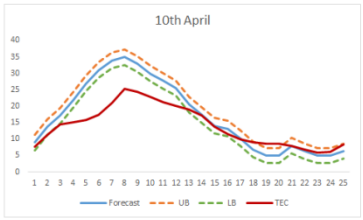

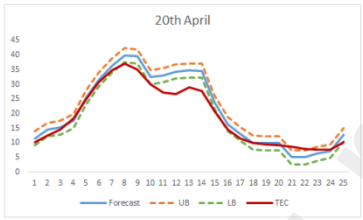

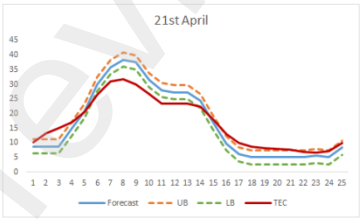

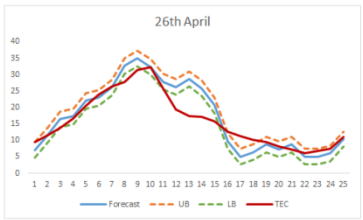

Identification of anomolous behaviour of TEC using Statistical ARIMA model

UB = Forecasted Value + 1.34 * Standard Deviation

LB = Forecasted Value - 1.34 * Standard Deviation

Table1. Three strong earthquakes that occurred in N-E India during the study time period.

Sl. No.	Date	Latitude (°N)	Longitude (°E)	Depth	Magnitude	Location
1.	13.04.2016	23.09	94.86	136	6.9	Eastern boundary zone
2.	17.11.2017	29.83	94.98	8	6.4	Mishmi Himalayan zone
3.	28.04. 2021	26.78	92.45	34	6.0	Dhekiajul, Assam

Table 2. Fractal correlation dimension according to fifty event windows with respect to mean time period.

Sl. No.	Dc (Correlation Dimension)	Mean Time of each 50 events (in month)	R^2 (Correlation coefficient)	Error(±) in D_c value	Highest Magnitude	Time period (when the Dc value is lower)
1	1.2584	2.65	0.9925	0.0075	6.1	
2	0.7418	6.41	0.9936	0.0064	5.2	27.12.2014 to 12.08.2015
3	1.4930	9.91	0.9902	0.0098	6.7	
4	1.4261	13.59	0.9950	0.0050	6.9	
5	1.4960	17.95	0.9926	0.0074	5.7	
6	1.1010	20.91	0.9909	0.0091	6.4	21.07.2017 to 18.01.2018
7	1.4164	25.97	0.9912	0.0088	5.2	
8	1.4299	30.05	0.9965	0.0035	5.9	
9	0.6728	34.01	0.9857	0.0143	5.5	03.07.2019 to 04.03.2020
10	0.7178	36.32	0.9906	0.0094	5.9	05.03.2020 to 24.07. 2020
11	0.3211	38.07	0.9732	0.0268	5.5	24.07.2020 to 08.11.2020
12	0.9643	41.18	0.9905	.0095	6	10.11.2020 to 18.05.2021
13	1.0035	42.54	0.9789	0.0211	6.1	18.05.2021 to 24.08.2021